



An Analytical Microcrack-Based Rock Model with Implications for Earthquake Mechanisms Induced by Stress Changes

Xiaozhao Li^{1,2,3} · Chengzhi Qi^{1,2} · Liren Ban^{1,2} · Zhushan Shao³

Received: 31 May 2019 / Accepted: 10 February 2020 / Published online: 2 March 2020
© International Association for Mathematical Geosciences 2020

Abstract Shear fracture triggered by subcritical crack extension in intact brittle rocks under long-term compressive loading plays a significant role in the evaluation of earthquake mechanisms. Changes in external loading strongly influence the subcritical crack growth of intact rocks during earthquake nucleation. An important conundrum is how to establish the relationship between shear fracture induced by subcritical crack growth and external loading path in brittle rocks under lithospheric conditions. A novel micromechanical method that introduces shear fracture behavior is proposed to predict the time-dependent shear properties induced by the subcritical cracking of brittle rocks when the initial state of rocks starts from the peak point of the stress–strain curve measured by the conventional triaxial compressive test. This approach is developed on the basis of the wing crack model, subcritical crack growth law, and Mohr–Coulomb strain-softening model. The effect of loading and unloading paths on the evolution of shear properties of rocks under lithospheric conditions is analyzed by drawing a function of historical stress. The corresponding evolution of strain, shear strength, cohesion, and internal friction angle caused by subcritical crack growth under different stress paths is studied. Cohesion and shear strength continuously undergo a weakening process, and the internal friction angle initially undergoes a strengthening and, finally, a weakening process during subcritical crack growth under constant compressive loadings. The effect of the sudden change in axial stress on shear strength is

✉ Xiaozhao Li
lixiaozhao@bucea.edu.cn

¹ School of Civil and Transportation Engineering, Beijing University of Civil Engineering and Architecture, Beijing 100044, China

² Beijing Advanced Innovation Center for Future Urban Design, Beijing 100044, China

³ Shaanxi Key Laboratory of Geotechnical and Underground Space Engineering, Xi'an University of Architecture and Technology, Xi'an 710055, Shaanxi, China

smaller than that of the sudden change in confining pressure. A sudden decrease in confining pressure causes a rapid drop in shear strength, leading to a dramatic rise and drop in the rate of shear strength. Implications for evaluating earthquake mechanisms triggered by stress changes from the evolution of shear properties caused by subcritical crack growth in brittle rocks are also proposed.

Keywords Rock mechanics · Shear fracture · Creeping crack growth · Stress change · Seismic mechanisms

1 Introduction

The shear properties of friction in rock faults (Scholz 1998; Daniels and Hayman 2008; Boneh et al. 2014; Niemeijer and Vissers 2014) and fracture in intact rocks (Ohnaka 1995; Katz and Reches 2004; Svetlizky and Fineberg 2014; Brantut and Viesca 2015) have been widely studied. The shear properties measured by friction and fracture are important for evaluating earthquake mechanisms.

Laboratory experiments on rocks containing artificial faults (Fig. 1a) have provided considerable insight into the mechanics of crustal earthquakes. Stable (or slow) sliding and stick (or fast) slip have been observed in artificial faults, which were studied using the rate- and state-dependent friction laws proposed by Dieterich (1979a, b) and Ruina (1983). Figure 1c, b shows the variation in shear stress, along with slip displacement and slip time, to clearly illustrate the rate- and state-dependent friction laws, respectively. Many studies have investigated the stable and unstable evolution of slip friction in faults, providing support for the study of earthquake mechanisms. Stable creeping slip plays an important role in earthquake nucleation, which can lead to a destructive result due to dynamic weakening. Unstable episodic sliding (or stick slip) consists of a relatively long period during which no slip occurs, shear stress increases, and an abrupt onset of fast slip with a stress drop is observed (Fig. 1b). The unstable process of stick-slip friction is closely related to the unstable earthquake process in faults (Rice and Ruina 1983; Douglas et al. 2005; Noda and Lapusta 2013; Dragoni and Lorenzano 2017). Fault asperities also have a crucial influence on earthquake nucleation and generation. The effects of the distribution and size of asperities on the mechanical properties along the faults have been widely studied (Ruff 1992; Rice 1993; Somerville et al. 1999; Dragoni and Tallarico 2016). The slow earthquake mechanism, in which the episodic tremor recorded by weak seismic signals accompanies the slow slip on faults, has also been proposed (Amoruso et al. 2004; Shelly et al. 2011; Ikari et al. 2013; Crampin et al. 2015; Leeman et al. 2016). Tremor and slow stick slip are induced by minor variations in stress from the ocean or solid earth tides, showing that changes in stress significantly influence the slow earthquake mechanism (Houston 2015).

The shear failure of rocks has been studied via the frictional slip along a fault under compressive conditions. However, apart from shear failure from frictional slip along a preexisting fault, the shear failure of rocks include the shear fracture of initially intact rocks (Ohnaka 1995). Ohnaka (1995) established a law describing the shear failure of intact rocks under the triaxial compressive test that simulates lithospheric conditions

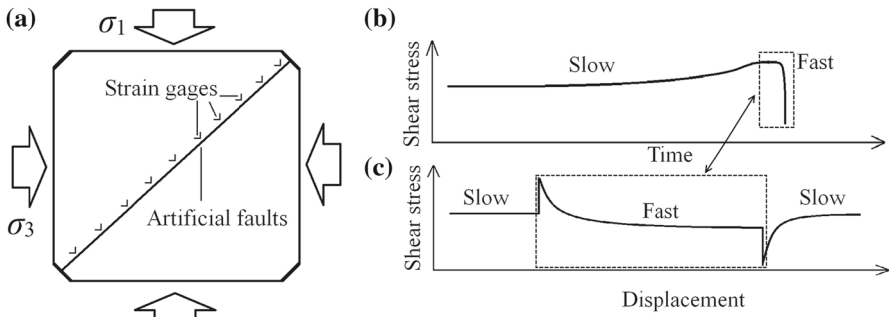


Fig. 1 **a** Schematic of rock friction experiment along artificial faults, **b** relationship between shear stress and time along the fault under compression, and **c** relationship between shear stress and displacement along the fault under compression (which is related to the rate- and state-dependent friction laws) (Dieterich 1979a, b)

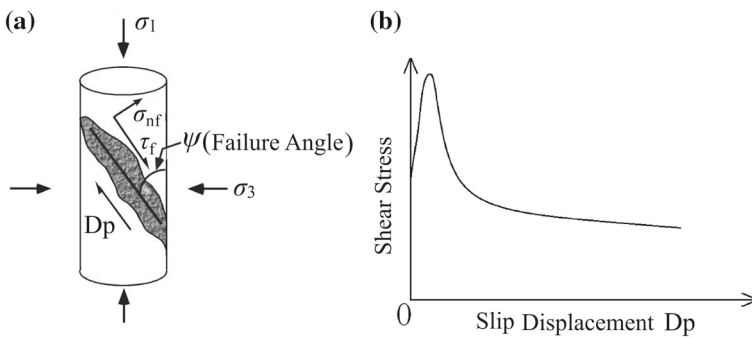


Fig. 2 **a** Configuration of shear fracture in an intact rock sample and **b** relationship between shear stress and slip displacement of intact brittle rocks under lithospheric conditions (Ohnaka 1995)

(Fig. 2a). This proposed law provides crucial help for judging the shear fracture behavior of intact rocks during earthquake nucleation. The relationship between resolved shear stress and displacement along the failure plane is shown in Fig. 2b. The shear stress initially increases to a peak value and then decreases with increasing deformation. This phenomenon is similar to the relation between shear stress and displacement shown in Fig. 1c. Ohnaka (1995) proposed a unified constitutive law to explain the shear failure from rock friction in preexisting faults and rock fracture in intact rocks. The frictional strength along the faults is equivalent to the shear fracture strength of intact rocks under the earth’s deep crust.

The phenomenological mechanism of earthquakes is widely accepted in the aforementioned references. Nevertheless, an underlying mechanism based on tensile microcrack growth of rocks provides further understanding of the earthquake mechanism (Crampin et al. 1984; Lockner et al. 1991; Beeler 2004; Healy et al. 2006; Griffith et al. 2009). Beeler (2004) also presented a constitutive model for brittle faulting caused by crack growth. This model consisted of two rheological components, namely, a stable deformation from subcritical crack growth and an unstable defor-

mation from crack coalescence and supercritical crack growth. The time-dependent shear failure behavior of rock fracture was consistent with rock friction according to laboratory observations. The two time-dependent shear failure behaviors agreed with the description by this crack-growth-based constitutive model. The behaviors were also similar to the predictions of the rate- and state-dependent laws (Dieterich 1979a, b) for the onset of rapid slip along a preexisting fault. The brittle microcrack growth in solid rock governs the nucleation process. The nucleation of shear rupture is a fracturing process, not a frictional one, and the coupling between friction and fracture is important for the evaluation of earthquake dynamics (Svetlizky and Fineberg 2014). The process of fault cementation, such as an inverse process of the fracturing process in intact rocks, likewise has an important role in evaluating earthquake nucleation, and the variation in microstructure between faults strongly influences the cementation processes (Tueckmantel et al. 2010; Fossen et al. 2011; Pei et al. 2015). The variations in density and distribution of microcracks in rocks are possible driving mechanisms for most earthquake precursors (Scholz et al. 1973; Byerlee 1978). A physical basis for earthquake precursors was proposed using the mechanical behavior of deformation and changes in wave velocity caused by microcrack growth in rocks (Aggarwal et al. 1973). In addition, geometrical variations in stress-aligned microcracks were observed through variations in shear-wave splitting for brittle rocks under the earth's crust. Variations in shear-wave splitting implying stress accumulation and relaxation were analyzed and observed in rocks prior to large earthquakes (Bianco et al. 2006; Crampin et al. 2015). During construction in deep underground engineering projects, excavation-induced changes in the initial conditions (pore fluid pressure, temperature, or stress state) around the underground rocks cause localized microcrack variations and the phenomena of microseismicity in rocks (Pearson 1981; Hatzfeld et al. 1999; Xiao et al. 2017; Colombero et al. 2018; Cao et al. 2018; Yu et al. 2020). Microseismicity is also important for evaluating and predicting the stability and safety of underground engineering. These studies provide an important framework for verifying the rationality of using the time-dependent shear strength of intact rocks to evaluate the process of earthquake nucleation in our study.

However, the earthquake mechanism caused by microcrack growth during long-term geological development has rarely been studied in a micromechanical model. The correlation between shear properties and microcrack growth in brittle rocks under lithospheric conditions has not been clearly established. Many studies modeling the micromechanics of rocks have focused on the evolution of deformation during creep (Miura et al. 2003; Brantut et al. 2012; Li and Shao 2016). The microcrack growth of brittle rocks during creep was likewise studied by acoustic emission and scanning electron microscopy (Grgic and Amitrano 2009), and minor changes in stress were found to cause significant changes in creep failure time. An analytical method was proposed to study the influence of step loading and unloading on creep deformation caused by microcrack growth (Li and Shao 2016), and a relationship between microcrack extension and shear properties was noted (Li et al. 2018a, b). However, the effect of stress changes on the evolution of shear properties with respect to the earthquake mechanism has not been clearly established.

The purpose of the present study is to establish a micromechanics-based method for investigating the influence of the stress path on the shear properties triggered by

subcritical crack growth in intact rocks. The proposed method is devised by coupling the wing crack model (Ashby and Sammis 1990), the law of subcritical crack growth (Charles 1958), Mohr–Coulomb strain-softening law (Zhao and Cai 2010), and a function of stress path. The evolution of rock deformation and shear strength caused by subcritical crack growth is studied in detail under different stress paths. New implications for evaluating earthquake mechanisms triggered by stress changes are presented via the analytical evolution of shear strength from microcrack growth in intact rocks.

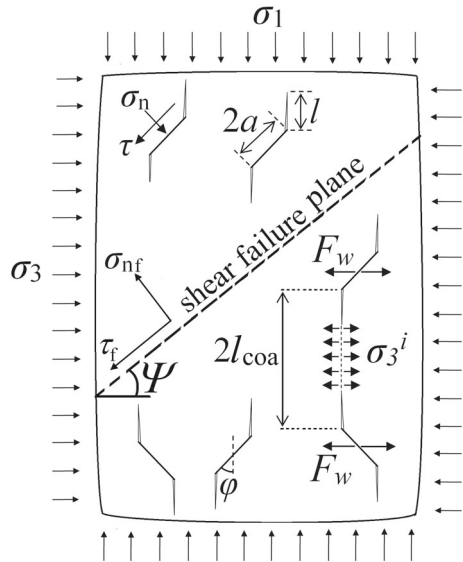
2 Formulation of Analytical Methods

An analytical microcrack-triggered model for evaluating the shear fracture of brittle rocks under compressive loadings is presented in Fig. 3. The model combines the Ashby and Sammis (1990) crack model and the Mohr–Coulomb strain-softening law (Zhao and Cai 2010). It is postulated as an isotropic elastic body. The fracture triggered by strain localization is investigated by a global fracture. In the model in Fig. 3, σ_1 and σ_3 are the axial stress and confining pressure, respectively, and $\sigma_3 = \sigma_2$; a is the initial crack size, l is the wing crack length, φ is the initial crack inclination, F_w is the wedge force on the initial crack plane, and σ_3^i is the internal stress between the tips of the wing crack. σ_n and τ are the normal and shear stress on the plane of the initial crack, respectively, τ_f and σ_{nf} are the shear strength and normal stress on the plane of the shear fracture, respectively, and ψ is the inclination of the shear fracture plane. The internal stress σ_3^i greatly influences the evaluation of the crack interaction-triggered rock fracture. The length of crack coalescence is $l_{coa} = (3/4\pi N_V)^{1/3} - \alpha a$ (Brantut et al. 2012), where α is the cosine of the crack inclination angle φ . The initial damage of the model is $D_0 = 4\pi N_V(\alpha a)^3/3$, where N_V is the initial crack number per unit volume. In this model, N_V is assumed to remain constant with an increase in damage. The rocks fails when the initial damage D_0 exceeds a threshold value. The approximate threshold value can be calibrated using the experimental data from scanning electron microscopy and the analytical data from this model. Rock damage D increases with wing crack growth, and $D = 4\pi N_V(l + \alpha a)^3/3$.

The existence of microcracks causes damage in solid materials and has a considerable effect on the mechanical behavior of such materials. In fracture mechanics theory, the crack effect on materials is described by the mechanical properties near the crack (e.g., stress intensity factor at crack tips). The stress intensity factors of different crack types subjected to various loading types were studied widely. On the basis of the factor of stress intensity defined by Ashby and Sammis (1990), the stress–crack relationship describing the crack hardening and softening phases (which correspond respectively to the strain hardening and softening phases) (Brantut et al. 2012; Li and Shao 2016) can be obtained as follows

$$\sigma_1(l) = \frac{\sigma_3[c_3(l) + A_2(c_1(l) + c_2(l))] - K_{IC}/\sqrt{\pi a}}{A_1[c_1(l) + c_2(l)]}, \quad (1)$$

Fig. 3 Model of shear failure related to microcrack extension in compression



where

$$c_1 = (l/a + \beta)^{-3/2} / \pi^2, \tag{2}$$

$$c_2 = 2\pi^{-2} \sqrt{l/a} / [\alpha^2 D_o^{-2/3} - (\alpha + l/a)^2], \tag{3}$$

$$c_3 = 2\sqrt{l/a} / \pi, \tag{4}$$

$$A_1 = \pi \sqrt{\beta/3} [\sqrt{1 + \mu^2} - \mu], \tag{5}$$

$$A_2 = A_1 (\sqrt{1 + \mu^2} + \mu) / (\sqrt{1 + \mu^2} - \mu), \tag{6}$$

and K_{IC} is the fracture toughness, and μ is the crack friction coefficient. Parameter β is a correction factor that calibrates the stress intensity factor at the wing crack length equal to 0. A peak stress σ_{1peak} can be obtained in Eq. (1), which corresponds to a peak crack length l_{peak} . On the basis of this peak point and the Mohr–Coulomb failure criterion, the correlation of crack parameters and shear failure properties at low confining pressures was proposed as follows (Li et al. 2016)

$$\tau_f(l = l_{peak}) = \sigma_{nf} (\tan \phi(l)) - c(l), \tag{7}$$

where

$$\sigma_{nf}(l = l_{peak}) = \frac{\sigma_{1peak} + \sigma_3}{2} + \frac{\sigma_{1peak} - \sigma_3}{2} \cos 2\psi(l), \tag{8}$$

$$\phi(l = l_{peak}) = 90^\circ - 2 \arctan \sqrt{\frac{A_1 (c_1(l) + c_2(l))}{c_3 + A_2 (c_1(l) + c_2(l))}}, \tag{9}$$

$$c(l = l_{\text{peak}}) = \frac{K_{\text{IC}}}{2\sqrt{A_1\pi a[c_3(l) + A_2(c_1(l) + c_2(l))]}(c_1(l) + c_2(l))}, \tag{10}$$

c and ϕ are the cohesion and internal friction angles, respectively; ψ is the inclination angle of the failure plane in Fig. 3, and $\psi = 45^\circ + \phi/2$. Equation (7) only explains the relationship between shear strength in the Mohr–Coulomb failure criterion and microcrack parameters at the peak point of Eq. (1). However, in the Mohr–Coulomb strain-softening law (Zhao and Cai 2010), the locus of the peak point at the cyclic compressive test is approximately equivalent to the post-peak curve of the stress–strain constitutive curve from the conventional compressive loading test, which helps in the evaluation of continuous shear properties at the post-peak phase of the stress–strain relation. A microcrack extension-based stress–strain constitutive relation describing the strain hardening and softening phases was obtained as well (Li et al. 2016), and this stress–strain relation corresponds to the relationship between stress and cracking in Eq. (1). Therefore, the peak stress locus is described by the post-peak correlation of stress and crack extension in Eq. (8). The invariant l_{peak} and $\sigma_{1\text{peak}}$ in Eqs. (7) to (10) are replaced respectively with the variables l and $\sigma_1(l)$ in the case of $l \geq l_{\text{peak}}$ (which corresponds to the case of $\varepsilon \geq \varepsilon_{1\text{peak}}$). In addition, the crack-dependent shear strength at the post-peak relation between stress and crack extension in Eq. (1) (i.e., $l \geq l_{\text{peak}}$) can be obtained as

$$\tau_f(l) = \sigma_{\text{nf}}(\tan \phi(l)) - c(l), \quad (l \geq l_{\text{peak}}), \tag{11}$$

where

$$\sigma_{\text{nf}}(l) = \frac{\sigma_1(l) + \sigma_3}{2} + \frac{\sigma_1(l) - \sigma_3}{2} \cos 2\psi(l), \tag{12}$$

$$\phi(l) = 90^\circ - 2\text{arc tan} \sqrt{\frac{A_1(c_1 + c_2)}{c_3 + A_2(c_1 + c_2)}}, \tag{13}$$

$$c(l) = \frac{K_{\text{IC}}}{2\sqrt{A_1\pi a [c_3 + A_2(c_1 + c_2)]}(c_1 + c_2)}, \tag{14}$$

and the inclination angle of the shear fracture plane $\psi(l) = \phi(l)/2 + 45^\circ$.

The axial strain related to wing cracking under the lower confining pressure, that is, $\varepsilon_1 = \varepsilon_o \{ - \ln[1 - [l/(\alpha a) + 1]^3 D_o] \}^{1/m}$ (Li et al. 2016), is substituted into Eqs. (11) to (14), and the strain-related shear strength, cohesion, and internal friction angle are derived as

$$\tau_f(\varepsilon_1) = \sigma_{\text{nf}}(\tan \phi(\varepsilon_1)) - c(\varepsilon_1), \quad (\varepsilon_1 \geq \varepsilon_{1\text{peak}}), \tag{15}$$

where

$$\sigma_{\text{nf}}(\varepsilon_1) = \frac{\sigma_1(\varepsilon_1) + \sigma_3}{2} + \frac{\sigma_1(\varepsilon_1) - \sigma_3}{2} \cos 2\psi(\varepsilon_1), \tag{16}$$

$$\phi(\varepsilon_1) = 90^\circ - 2\text{arc tan} \sqrt{\frac{A_1(Z_1 + Z_2)}{Z_3 + A_2(Z_1 + Z_2)}}, \tag{17}$$

$$c(\varepsilon_1) = \frac{K_{IC}}{2\sqrt{A_1\pi a(Z_3 + A_2(Z_1 + Z_2))(Z_1 + Z_2)}}, \tag{18}$$

$$Z_1 = \pi^{-2} (\alpha Z_4 + \beta)^{-3/2}, \tag{19}$$

$$Z_2 = \frac{2\pi^{-2}\alpha^{-3/2}Z_4^{1/2}}{D_0^{-2/3} - (Z_4 + 1)^2}, \tag{20}$$

$$Z_3 = 2\pi^{-1}\sqrt{\alpha Z_4}, \tag{21}$$

$$Z_4 = \left[\frac{1 - \exp[-(\varepsilon_1/\varepsilon_0)^m]}{D_0} \right]^{1/3} - 1, \tag{22}$$

$$\psi(\varepsilon_1) = 45^\circ + \phi(\varepsilon_1)/2. \tag{23}$$

When the factor of stress intensity in Ashby and Sammis (1990) and the law of subcritical crack growth (Charles 1958) are combined, the evolution of subcritical crack growth induced by stress changes is obtained as follows (Li and Shao 2016)

$$\frac{dl}{dt} = v(\pi a)^{n/2} \left\{ \frac{[A_2\sigma_3(t) - A_1\sigma_1(t)](c_1 + c_2) + \sigma_3(t)c_3}{K_{IC}} \right\}^n, \tag{24}$$

where v is the characteristic velocity of the crack extension, and n is the index of stress corrosion. An initial length of wing crack l_0 can be achieved by inserting an initial stress state (σ_1, σ_3) into Eq. (1). The initial axial stress is larger than the stress of crack initiation and smaller than the rock strength at the given value of confining pressure. This initial value of wing crack is the initial iteration value of Eq. (24). Numerical results for the time-dependent wing crack extension [i.e., $l(t)$] can be obtained. The time-dependent axial strain corresponds to the time-dependent wing cracking on the rock, which is obtained by inserting Eq. (24) into the strain–crack relation $\varepsilon_1 = \varepsilon_0 \{ -\ln[1 - [l/(\alpha a) + 1]^3 D_0] \}^{1/m}$ (Li and Shao 2016).

For the case of $l \geq l_{peak}$, the time-dependent crack extension [i.e., $l(t)$] can be solved by introducing l_{peak} as the initial iteration value of the crack extension (i.e., $l_0 = l_{peak}$) for the numerical integration of Eq. (24). l_{peak} is obtained by the crack–stress relation of Eq. (1) under the given value of the initial stress state. Substituting this time-dependent crack extension into Eqs. (11) to (14) can achieve the evolution of shear strength under different stress paths as follows

$$\tau_f(t) = \sigma_{nf}(\tan \phi(t)) - c(t), \tag{25}$$

where

$$\sigma_{nf}(t) = \frac{\sigma_1(t) + \sigma_3(t)}{2} + \frac{\sigma_1(t) - \sigma_3(t)}{2} \cos 2\psi(t), \tag{26}$$

$$\phi(t) = 90^\circ - 2 \arctan \sqrt{\frac{A_1(c_1(t) + c_2(t))}{c_3(t) + A_2(c_1(t) + c_2(t))}}, \tag{27}$$

$$c(t) = \frac{K_{IC}}{2\sqrt{A_1\pi a [c_3(t) + A_2(c_1(t) + c_2(t))](c_1(t) + c_2(t))}}, \tag{28}$$

$$\psi(t) = 45^\circ + \frac{\phi(t)}{2}. \quad (29)$$

Crack growth at the closed crack is caused by the sliding of the initial crack after shear stress overcomes the friction force between crack interfaces. Crack growth at the pore is caused by the stress concentrations around the pore (Ashby and Sammis 1990). If the closed crack is regarded as an open crack (which is approximately equivalent to the pore neglecting the effects of the geometrical shape of micro-defects), then the friction coefficient is neglected (i.e., $\mu = 0$), which provides an approximate understanding of the mechanical behavior of porous rocks on the basis of the proposed model.

3 Results and Discussion

3.1 Quasi-Static Variations in Shear Properties with Crack Growth or Axial Strain During Post-Peak Failure

Table 1 shows the model parameters in this study. These parameters are used to validate the rationality of theoretical stress–strain curves that describe the strain hardening and softening phases and creep curves that describe the decelerated, steady-state, and accelerated phases of rocks (Li and Shao 2016). The variations in shear strength, cohesion, and internal friction angle from microcrack growth of brittle rock appearing at the post-peak phase of quasi-static failure are shown in Fig. 4a. The figure provides an understanding of shear behavior caused by microcrack growth. However, the crack growth-dependent shear strength, cohesion, and internal friction angle are not macroscopically observed and measured in conventional compressive tests. To clearly and directly verify the rationality of the presented analytical method, a macroscopic description of the relationship among shear strength, internal friction angle, cohesion, and axial strain is shown in Fig. 4b. At the post-peak phase of the axial stress–strain curve, shear strength and cohesion continuously weaken with increasing axial strain caused by crack growth, and the internal friction angle initially strengthens and then weakens with increasing axial strain caused by crack growth, consistent with the experimental results under triaxial compressive loadings (Martin and Chandler 1994).

Many studies have noted that the phenomenon observed in the onset of shear fracture in intact rocks is similar to that in the onset of rapid slip along a preexisting fault in rate- and state-dependent laws (Dieterich 1979a, b; Ruina 1983). The underlying physical process in the onset of shear fracture is the same as that in the onset of earthquakes (Brace and Byerlee 1966; Ohnaka 1995; Beeler 2004). Thus, the variation in shear strength with deformation (i.e., axial strain) in Fig. 4b is similar to the variation in shear stress with deformation (slip displacement) during fast slip in Figs. 1 and 2. A direct comparison of the results of the proposed method with published data (Dieterich 1979a, b; Ruina 1983; Ohnaka 1995) on the relationship between normalized shear stress and normalized deformation is shown in Fig. 5. The difference between the two results may be due to some average assumptions for the case of the microcrack geometries and distribution in the proposed model. However, the rate- and state-dependent laws in

Table 1 Model parameters in this study

Parameters	Values
Fracture toughness, K_{IC} (MPa m ^{1/2})	1.61
Corrosion index, n	57
Characteristic crack velocity, v (m/s)	0.16
Constant of materials, m	1.0
Constant of materials, ϵ_0	0.0147
Crack angle, ϕ	45°
Friction coefficient, μ	0.51
Radius of initial crack, a (mm)	3.1
Correction factor, β	0.32
Initial damage, D_0	0.048

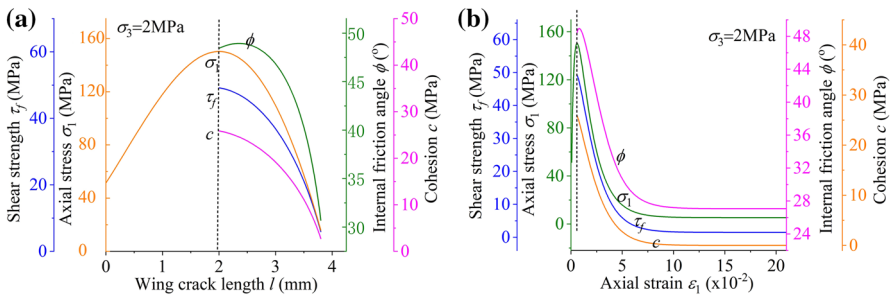


Fig. 4 Variations in axial stress, shear strength, internal friction angle, and cohesion along with **a** wing crack length and **b** axial strain

Fig. 5 Comparisons of the relationship between normalized shear stress and normalized deformation in this study, Dieterich (1979a, b), Ruina (1983), and Ohnaka (1995)

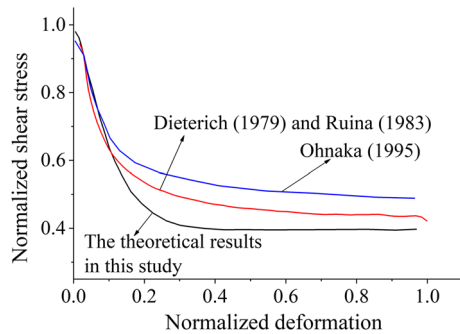


Fig. 1 can explain the effect of the sudden change in slip velocity on shear stress (i.e., the strengthening phase, where shear stress increases rapidly with slip displacement or time). However, our proposed model only explains shear fracture in intact rocks and cannot explain the effect of slip rate variation on shear strength.

These variations in shear properties are closely related to the stress-induced quasi-static crack growth and axial strain. Such sudden changes in applied stress cause the

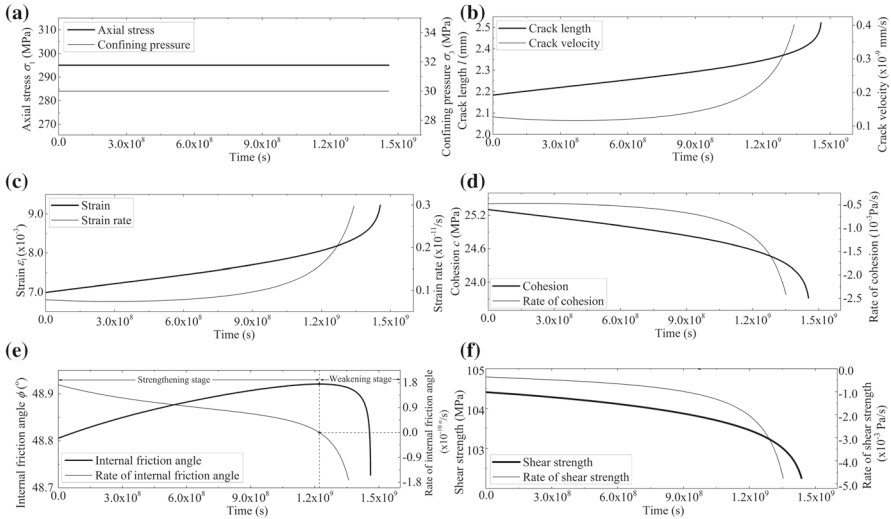


Fig. 6 Evolution and rate of **b** crack growth, **c** strain, **d** cohesion, **e** internal friction angle, and **f** shear strength under **a** constant axial stress and confining pressure

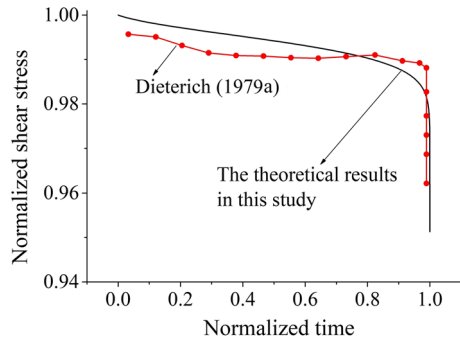
change in deformation and deformation rate, which may approximately explain the effect of the sudden change in slip velocity on shear stress under rate- and state-dependent laws (Dieterich 1979a, b; Ruina 1983).

3.2 Time-Dependent Static Crack Growth, Strain, and Shear Properties Under Constant Stress State

The evolution of crack growth, strain, and shear properties (i.e., internal friction angle, cohesion, and shear strength) of brittle rocks under a constant stress state (i.e., creep) is shown in Fig. 6, along with the corresponding rates of crack extension, strain, and shear properties. The crack initially experiences a slow accelerated growth, and then a rapid accelerated growth (Fig. 6b), which causes slow and rapid accelerated strain, respectively (Fig. 6c). Shear strength undergoes a slow and rapid accelerated weakening stage (Fig. 6f), which is attributed to cohesion that undergoes an accelerated weakening process (Fig. 6d) and the internal friction angle that initially undergoes a decelerated strengthening and subsequent accelerated weakening process (Fig. 6e).

Rock failure occurs at the rapid accelerated stage of crack growth and strain and the rapid accelerated weakening stage of internal friction angle, cohesion, and shear strength. Previous studies have rarely focused on the evolution of cohesion and internal friction angle in brittle rocks. Figure 6e shows that the transformation between the strengthening and weakening stages of the internal friction angle is clearly determined by the rate of internal friction angle and shear strength. The positive rate of internal friction angle represents the strengthening stage, and the negative rate represents the weakening stage. The time elapsed in the transformation between the strengthening

Fig. 7 Comparison of study results for time-dependent normalized shear stress in this study and in Dieterich (1979a). The normalized shear stress (or time) is defined by the division of the values between shear stress (or time) and maximum shear stress (or time)



and weakening stages of the internal friction angle is approximately 1.23×10^9 s (Fig. 6e).

Under quasi-static compression, the similarity between the onset of shear fracture in intact rocks in the proposed model and the onset of rapid slip along a preexisting fault in the rate- and state-dependent laws (Dieterich 1979a, b) is verified by comparing the variations in shear stress with deformation in intact rocks and faults in Fig. 5. Figure 1 also shows the variation in time-dependent shear stress during fast slip in the rate- and state-dependent laws for the quasi-static condition. The shear stress during fast slip decreases over time. However, if this quasi-static condition is replaced with a static condition, that is, the stress state remains constant, then the time-dependent shear strength is obtained in Fig. 6f.

The proposed results for the evolution of shear strength caused by microcrack growth in Fig. 6f are similar to the phenomenon of time-dependent shear stress during fast slip as described by Dieterich (1979a, b) and shown in Fig. 1. The normalized relation between shear stress and time owing to the difference at the scale of coordinate values is shown in Fig. 7. The initial state of time-dependent mechanical behavior is selected by the peak point of the stress–strain relationship in Fig. 4b. The applied stress at the post-peak phase of the stress–strain curve is also equivalent to the rock strength (Zhao and Cai 2010). Thus, the shear strength in this study is equivalent to the shear stress obtained experimentally by Dieterich (1979a).

Therefore, our study results for the evolution of shear strength in intact rocks have significant implications for evaluating the process of earthquake nucleation in the earth’s crust on the basis of micromechanics. In the process of earthquake nucleation, the time-dependent stable and unstable deformations from rock fracture are controlled by the physical process of crack growth (Beeler 2004; Svetlizky and Fineberg 2014). Stable deformation generates a small inelastic strain caused by subcritical crack growth, which corresponds to the steady-state crack growth (Fig. 6b), creep strain (Fig. 6c), evolution of cohesion (Fig. 6d), evolution of internal friction angle (Fig. 6e), and evolution of shear strength (Fig. 6f). Unstable deformation (i.e., rapid slip) generates a large strain caused by crack coalescence and supercritical crack growth, which corresponds to accelerated crack growth (Fig. 6b) and creep strain (Fig. 6c), and the drop in cohesion (Fig. 6d), internal friction angle (Fig. 6e), and shear strength (Fig. 6f).

The environment of rocks subjected to a constant stress state is approximately equivalent to the case of lithospheric conditions. This finding provides implications for the occurrence of regular earthquakes on the basis of the shear failure of intact rocks caused by microcrack growth.

The effects of initial crack size, friction coefficient, confining pressure, and initial damage on the evolution of cohesion, internal friction angle, and shear strength are also investigated and are presented in Fig. 8. As shown in Fig. 8a to c, when the initial crack number N_V is given as 1.3×10^6 , the final time at the drop in cohesion, internal friction angle, and shear strength decreases with the increase in initial crack size. As shown in Fig. 8d to f, the final time at the drop in cohesion, internal friction angle, and shear strength increases with the increase in friction coefficient between crack interfaces. As shown in Fig. 8g to i, the final time at the drop in cohesion, internal friction angle, and shear strength increases with the increase in confining pressure. The internal friction angle and cohesion change slightly under different confining pressures over a given time because of the irrelevance of the internal friction angle, cohesion, and confining pressure in Eqs. (13) and (14). Shear strength increases with the increase in confining pressure over a given time. In Fig. 8j to l, the final time at the drop in cohesion, internal friction angle, and shear strength increases with the decrease in initial damage. The internal friction angle, cohesion, and shear strength decrease with the increase in initial damage in a given time.

A small change in model parameters (i.e., initial crack size, friction coefficient, confining pressure, or initial damage) likewise causes a time variation over several orders of magnitudes. This phenomenon shows that the changes in internal rock properties or external effect factors have a significant influence on the rock fracture process during creep deformation.

The evolution of strain, cohesion, internal friction angle, and shear strength is closely related to the subcritical crack growth of brittle rocks. The initial state of the rocks is selected by the peak point of the stress–strain relationship (which corresponds to the relationship between crack growth and stress) in Fig. 4.

3.3 Effects of Stress Changes on the Evolution of Crack Growth, Strain, and Shear Properties

Changes occur in the stress applied to rocks in the earth's crust due to the geological tectonic development induced by different factors (e.g., ocean or solid earth tides), which influence the slow earthquake mechanism. This mechanism, in which the episodic tremor recorded by weak seismic signals accompanies slow slip on faults, has been presented in a number of studies (Shelly et al. 2011; Crampin et al. 2015; Leeman et al. 2016). Tremor and slow stick slip are caused by minor stress variations from the ocean or solid earth tides (Houston 2015). Thus, the evolution of rock deformation and shear strength triggered by stress changes has important implications for the evaluation of the slow earthquake mechanism (Hardebeck et al. 1998; Belardinelli et al. 2003). In the analyses, the initial axial stress is selected as 295 MPa, and the initial confining pressure is selected as 30 MPa, thereby providing a qualitative comparison of the effects of different stress paths on time-dependent compressive-shear failure.

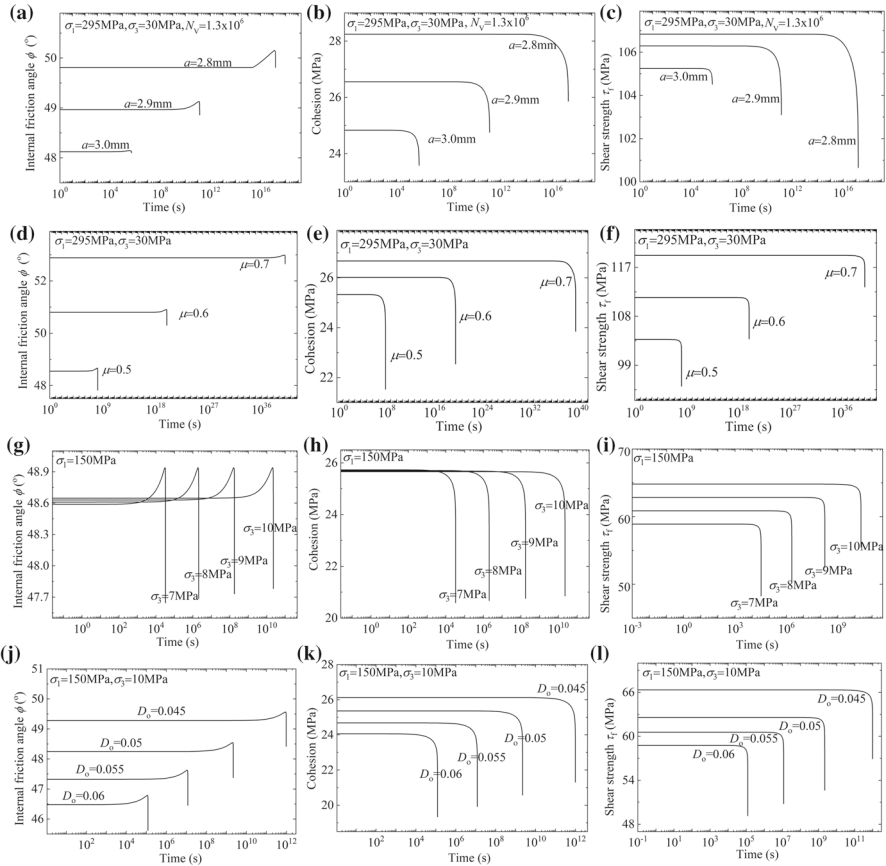


Fig. 8 Effects of **a–c** initial crack size a , **d–f** crack friction coefficient μ , **g–i** confining pressure σ_3 , and **j–l** initial damage D_0 on the evolution of cohesion, internal friction angle, and shear strength

Figure 9 shows the effects of step loading of axial stress on time-dependent crack growth, axial strain, cohesion, internal friction angle, and shear strength, along with the corresponding rates. Crack length and axial strain increase at a steady state in the two earlier steps and accelerate in the last step. Cohesion and shear strength decrease at a steady state in the two earlier steps and drop rapidly in the last step. The internal friction angle increases at a steady state in the two earlier steps and then decelerates and is then accompanied by an accelerated drop in the last step. The steady-state rates of crack growth, axial strain, cohesion, and shear strength increase with successive step numbers. The sudden rise in axial stress in each step in Fig. 9a causes step variations in the crack velocity, axial strain rate, rate of cohesion, rate of internal friction angle, and rate of shear strength.

Figure 10 shows the effects of step unloading of confining pressure on time-dependent crack growth, axial strain, cohesion, internal friction angle, and shear strength, along with the corresponding rates. Crack length and axial strain increase at a steady state during the earlier six steps and accelerate in the last step. Cohesion

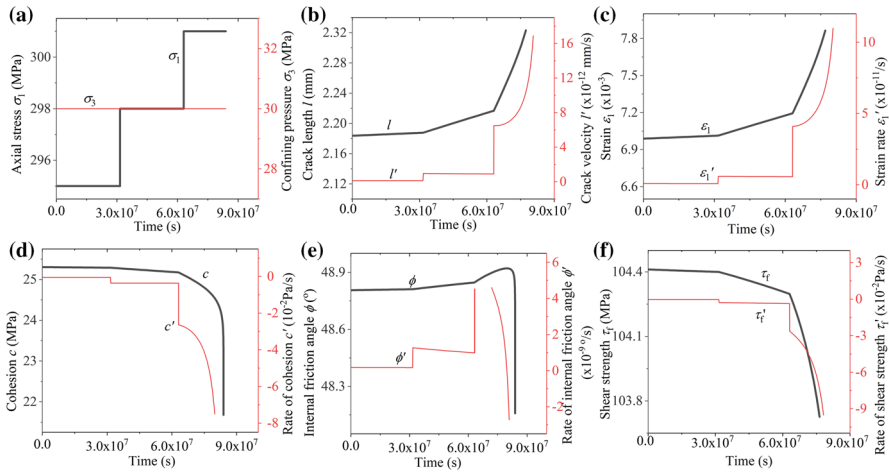


Fig. 9 Evolution and rate of **b** crack growth, **c** strain, **d** cohesion, **e** internal friction angle, and **f** shear strength under **a** step loading of axial stress and constant confining pressure

decreases at a steady state during the first six steps and drops rapidly in the last step. The internal friction angle increases at a steady state in the earlier six steps and decelerates initially and then drops rapidly in the last step. Shear strength decreases initially at a steady state and then drops slightly in each of the earlier steps, and finally shows a marked drop in the last step. A slight decrease in shear strength can cause a small earthquake, and a large decrease in shear strength can cause a large earthquake. The sudden drop in confining pressure in each step in Fig. 10a causes step variations in crack velocity, axial strain rate, rate of cohesion, and rate of internal friction angle. However, in Fig. 10f, the sudden rise in confining pressure causes a sudden rise in shear strength, leading to a large variation in the rate of shear strength. Therefore, the sudden change in confining pressure significantly influences shear strength.

A comparison between Figs. 9 and 10 and Fig. 6 shows that the final failure time at step loading of axial stress and confining pressure is shorter than that at a constant stress state ($\sigma_1 = 295$ MPa, $\sigma_3 = 30$ MPa). Thus, the step loading of axial stress and unloading of confining pressure accelerate rock failure and earthquake occurrence.

The evolution and rate of crack, strain, cohesion, internal friction angle, and shear strength subjected to increasing repeated loading and unloading of axial stress under constant confining pressure is shown in Fig. 11. The function in the path of axial stress is $\sigma_1 = 295$ MPa + $0.1 t - 3$ MPa $[t/T]$, cyclic time $T = 60 \times 60 \times 24 \times 365$ s, and $[t/T]$ represents the integralization for t/T (if $t/T = 0.6$, then $[t/T] = 0$; if $t/T = 8.9$, then $[t/T] = 8$).

Except for the phases of sudden drop in axial stress in Fig. 11a, the crack undergoes a slow accelerated growth during the earlier cycles and rapid accelerated growth in the last cycle. In addition, the minimum crack velocity in each cycle increases incrementally with the cycle number (Fig. 11b). The phenomenon of strain evolution (Fig. 11c) is similar to that of crack growth. Except for the phases of the sudden drop in axial stress, cohesion undergoes a slow accelerated weakening process during the

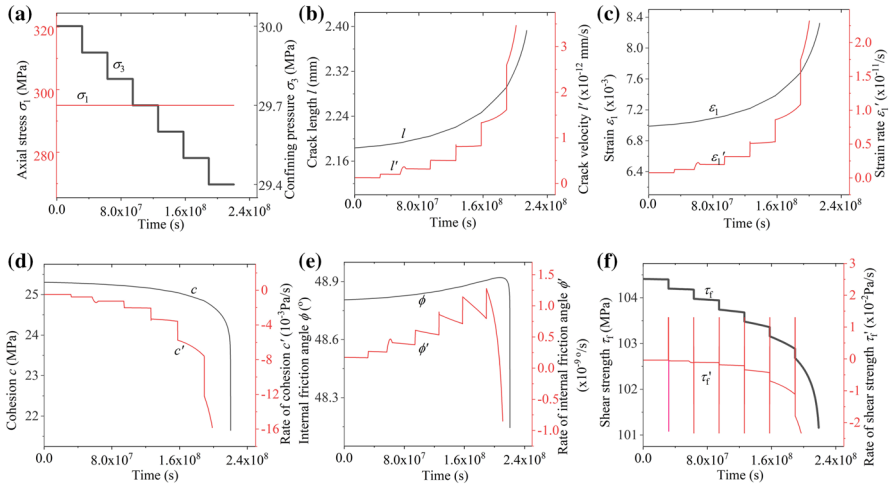


Fig. 10 Evolution and rate of **b** crack growth, **c** strain, **d** cohesion, **e** internal friction angle, and **f** shear strength under **a** step unloading of confining pressure and constant axial stress

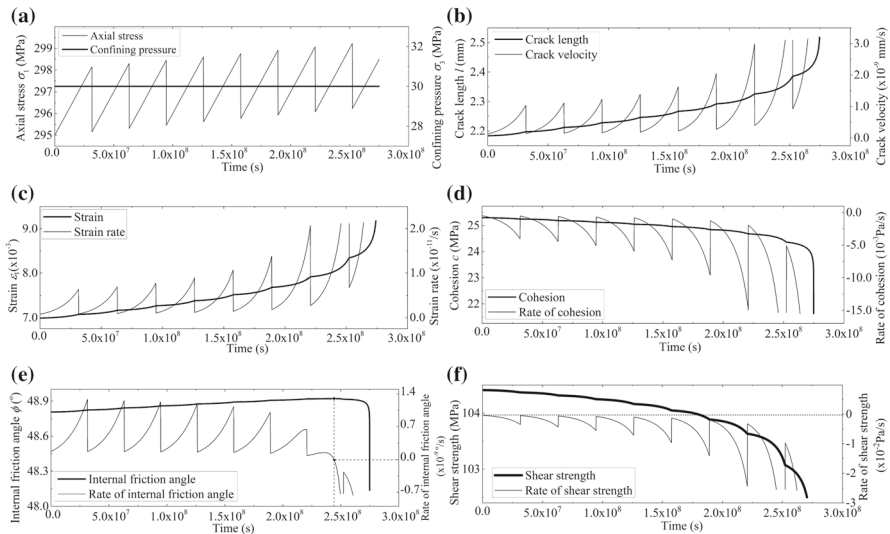


Fig. 11 Evolution and rate of **b** crack growth, **c** strain, **d** cohesion, **e** internal friction angle, and **f** shear strength under **a** increasing repeated loading and unloading of axial stress and constant confining pressure

earlier cycles, and a rapid drop in cohesion appears in the last cycle. The minimum rate of cohesion in each cycle increases incrementally with the cycle number (Fig. 11d). Except for the phases of sudden drop in axial stress, the internal friction angle undergoes a slow accelerated strengthening in most of the earlier cycles and an accelerated weakening process in the subsequent few cycles. A rapid drop in the internal friction angle appears in the last cycle. Before the internal friction angle enters the weakening stage (i.e., rate of internal friction angle is negative), it undergoes a transformation

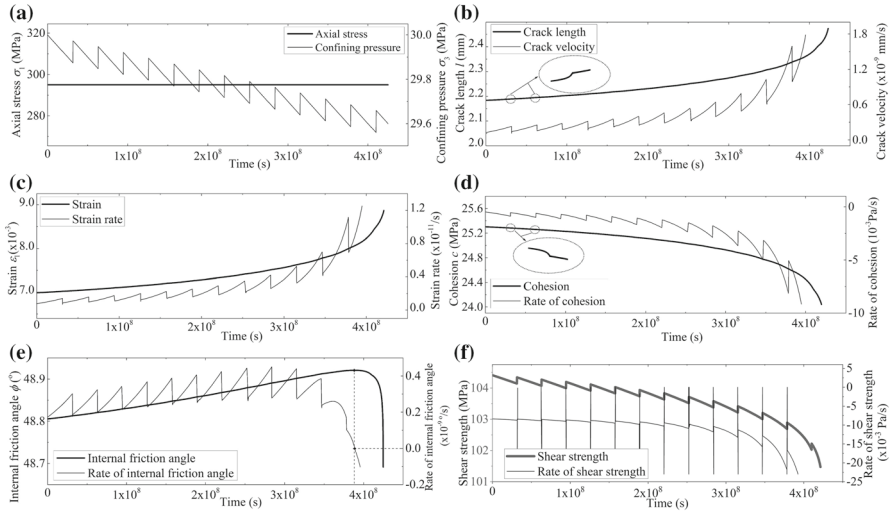


Fig. 12 Evolution and rate of **b** crack growth, **c** strain, **d** cohesion, **e** internal friction angle, and **f** shear strength under **a** decreasing repeated unloading and loading of confining pressure, and constant axial stress. The dashed circle indicates the enlargement area

from an accelerated strengthening stage to a decelerated strengthening stage (Fig. 11e). In Fig. 11f, except for the phases of sudden drop in axial stress, shear strength experiences a slow accelerated weakening during the earlier cycles and a rapid accelerated weakening process accompanied by a large drop in shear strength in the last cycle.

Figure 12 shows the evolution and rate of crack, strain, and shear properties under decreasing repeated unloading and loading of confining pressure, and constant axial stress. The function in the path of confining pressure is $\sigma_3 = 30 \text{ MPa} - 0.004 t + 0.1 \text{ MPa}$ [$t/(60 \times 60 \times 24 \times 365 \text{ s})$]. The phenomenon observed in the evolution of crack, strain, cohesion, internal friction angle, and shear strength is the same as that in the evolution of crack, strain, and shear properties under the increasing repeated loading and unloading of axial stress in Fig. 11. This finding shows that the mechanisms induced by increasing repeated loading and unloading of axial stress and decreasing repeated unloading and loading of confining pressure are similar. The sudden drop in axial stress shown in Fig. 11a and the sudden rise in confining pressure in Fig. 12a cause a deceleration in the evolution of crack length, axial strain, cohesion, internal friction angle, and shear strength. The continuous slow increase in axial stress in Fig. 11a and the continuous slow decrease in confining pressure in Fig. 12a accelerate the evolution of crack length, axial strain, cohesion, internal friction angle, and shear strength.

A comparison between Fig. 6 and Figs. 11 and 12 shows that the time of rock failure under repeated loading and unloading of axial stress or confining pressure is shorter than the time of rock failure under a constant stress state. The stress paths of increasing repeated loading and unloading of axial stress and decreasing repeated loading and unloading of confining pressure accelerate the crack growth. For earthquake mechanisms, the effect of increasing repeated loading and unloading of axial

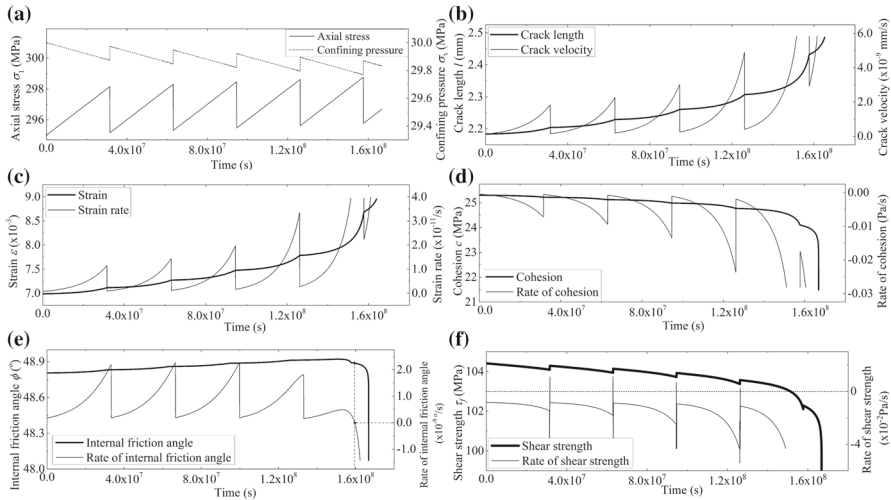


Fig. 13 Evolution and rate of **b** crack growth, **c** strain, **d** cohesion, **e** internal friction angle, and **f** shear strength under **a** increasing repeated loading and unloading of axial stress, and decreasing repeated unloading and loading of confining pressure

stress or decreasing repeated loading and unloading of confining pressure applied to rocks under lithospheric conditions accelerates the occurrence of an earthquake.

Figures 11 and 12 show the effect of increasing repeated loading and unloading of axial stress and decreasing unloading and loading of confining pressure, respectively. The coupling effect of increasing repeated loading and unloading of axial stress and decreasing unloading and loading of confining pressure is shown in Fig. 13. The path function of axial stress and confining pressure is equivalent to the function in Figs. 11 and 12, respectively. The evolution of crack, strain, and shear properties is similar to the phenomena in Figs. 11 and 12. A comparison between Fig. 13 and Figs. 11 and 12 shows that the time of rock failure with the coupling effect of axial stress and confining pressure is shorter than the time of rock failure with the single effect of axial stress or confining pressure. Therefore, the coupling effect of increasing repeated loading and unloading of axial stress and decreasing repeated loading and unloading of confining pressure applied to rocks under lithospheric conditions accelerates the crack growth to fracture of rocks and the occurrence of a regular earthquake.

Figure 14 shows the coupling effect of increasing repeated loading and unloading of axial stress and confining pressure on crack growth, strain, and shear properties. The function of the path of axial stress is $\sigma_1 = 295 \text{ MPa} + 0.1 t - 3 \text{ MPa} [t/(60 \times 60 \times 24 \times 365 \text{ s})]$, and the function of the path of confining pressure is $\sigma_3 = 30 \text{ MPa} + 0.004 t - 0.1 \text{ MPa} [t/(60 \times 60 \times 24 \times 365 \text{ s})]$. Except for the phases of sudden variation in axial stress and confining pressure, shear strength is always in a decelerated strengthening phase (i.e., rate of shear strength decreases and is larger than 0 at each cycle) in earlier cycles and undergoes an accelerated weakening phase in subsequent cycles. In addition, a rapid drop in shear strength occurs in the last cycle. The coupling effect of the sudden drop in confining pressure and axial stress causes a large drop in shear strength, which may cause a small earthquake. For each cycle, the increasing axial

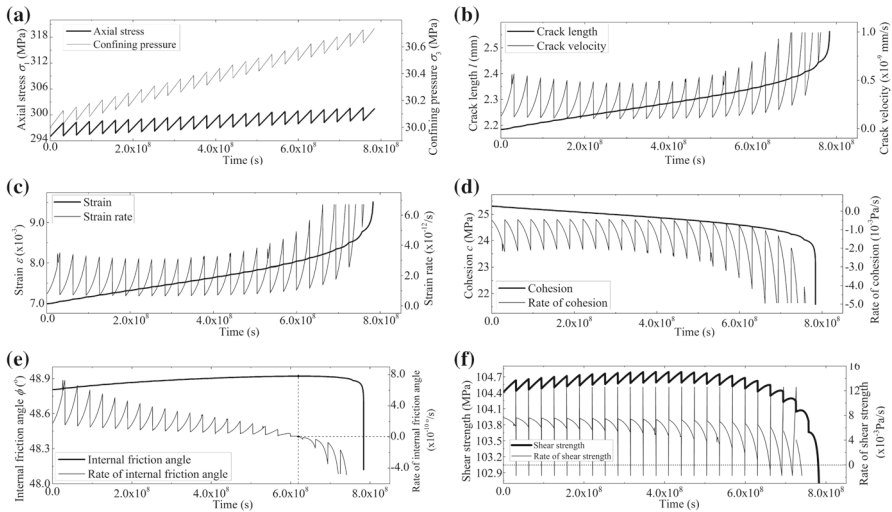


Fig. 14 Evolution and rate of **b** crack growth, **c** strain, **d** cohesion, **e** internal friction angle, and **f** shear strength under **a** increasing repeated loading of axial stress and confining pressure

stress dominates the accelerated variations in crack growth, axial strain, cohesion, and internal friction angle, and the sudden drop in axial stress dominates the sudden drop in crack velocity, strain rate, cohesion rate, and rate of internal friction angle. The slow increase in confining pressure dominates the decelerated strengthening shear strength, and the sudden drop in confining pressure dominates the sudden drop in shear strength.

Compared with Fig. 12, the increasing repeated loading and unloading of confining pressure in Fig. 14 causes a deceleration in crack growth, increase in the time of rock failure, and a slowing of the occurrence of an earthquake.

4 Conclusions

An analytical approach for studying the influence of the stress path on the evolution of shear strength from subcritical crack growth is proposed, which has new implications for the evaluation of earthquake mechanisms triggered by stress changes. The wing microcrack model, subcritical crack growth law, function of stress path, and Mohr–Coulomb strain-softening model are coupled in this method. The following conclusions are drawn:

1. In the post-peak phase of quasi-static stress–strain curves for brittle rocks, the internal friction angle initially increases to a maximum value and then decreases with further crack growth or increased strain. The cohesion and shear strength decrease with crack growth or increased strain.
2. For brittle rocks subjected to a constant stress state, crack growth and strain undergo slow acceleration and rapid acceleration stages, cohesion and shear strength experience a slow accelerated weakening stage and a rapid drop, and the internal friction angle undergoes decelerated strengthening and accelerated weakening stages. The

time-dependent shear strength is similar to the evolution of shear stress of brittle rocks during earthquake nucleation, which has implications for the evaluation of the regular earthquake mechanism.

3. In comparison with the failure time of rock under a constant stress state, the step loading of axial stress, step unloading of confining pressure, increasing repeated loading and unloading of axial stress, and decreasing repeated unloading and loading of confining pressure accelerate crack growth and rock fracture. The increasing repeated loading and unloading of confining pressure also causes a deceleration in crack extension and rock failure.
4. Under step loading of axial stress and step unloading of confining pressure, the internal friction angle undergoes a steady-state strengthening phase in earlier steps and a decelerated strengthening phase initially and then an accelerated weakening phase in the last step. Cohesion and shear strength experience a steady-state weakening phase in earlier steps and an accelerated weakening phase in the last step. Under the step unloading of confining pressure, shear strength initially decreases at a steady state and is then accompanied by a slight drop in the earlier step, and finally a large accelerated drop in the last step.
5. When subjected to the increase in repeated loading and unloading of axial stress or the decrease in repeated unloading and loading of confining pressure, the internal friction angle experiences a slow accelerated strengthening process in most of the early cycles and a rapid accelerated weakening process in the subsequent few cycles. In addition, cohesion undergoes an accelerated weakening in each cycle. Shear strength also undergoes a slow accelerated weakening process in most of the early cycles and a rapid accelerated weakening process accompanied by a drop in shear strength in the last cycle.
6. The effect of a sudden change in confining pressure on shear strength is greater than that of a sudden change in axial stress. The sudden increase or decrease in confining pressure causes a sudden rise or drop in shear strength, which gives rise to a large sudden increase or decrease in the rate of shear strength. This phenomenon of a drop in shear strength caused by stress changes is similar to the slow earthquake mechanism caused by minor variations in stress from various factors (e.g., ocean or solid earth tides).

However, the studies provide a simplified theoretical method for predicting earthquake mechanisms induced by stress changes from a shear fracture caused by the subcritical crack growth of brittle rocks. The failure from the strain localization of rocks is equivalently studied by the global failure of the wing crack model. In the time-dependent shear properties caused by subcritical crack growth, the initial state starts from the peak point of the stress–strain relation measured by the standard post-failure test. The rock can undergo long-term subcritical crack growth during the post-peak phase of the stress–strain relation.

Acknowledgements This work was supported by the National Natural Science Foundation of China (Grant No. 51708016), the Key Program for Shaanxi Key Laboratory of Geotechnical and Underground Space Engineering (Grant No. YT201902), the Fundamental Research funds for Beijing Universities (Grant Nos. X19006 and X19013), and the Program for Changjiang Scholars and Innovative Research Team in University (Grant No. IRT-17R06).

References

- Aggarwal YP, Sykes LR, Armbruster J, Sbar ML (1973) Premonitory changes in seismic velocities and prediction of earthquakes. *Nature* 241(241):101–104
- Amoruso A, Crescentini L, Dragoni M, Piombo A (2004) Fault slip controlled by gouge rheology: a model for slow earthquakes. *Geophys J Int* 159(1):347–352
- Ashby MF, Sammis CG (1990) The damage mechanics of brittle solids in compression. *Pure Appl Geophys* 133(3):489–521
- Beeler NM (2004) Review of the physical basis of laboratory-derived relations for brittle failure and their implications for earthquake occurrence and earthquake nucleation. *Pure Appl Geophys* 161:1853–1876
- Belardinelli ME, Bizzarri A, Cocco M (2003) Earthquake triggering by static and dynamic stress changes. *J Geophys Res* 108(B3):2135
- Bianco F, Scarfi L, Pezzo ED, Patanè D (2006) Shear wave splitting changes associated with the 2001 volcanic eruption on Mt Etna. *Geophys J Int* 167(2):959–967
- Boneh Y, Chang JC, Lockner DA, Reches Z (2014) Evolution of wear and friction along experimental faults. *Pure Appl Geophys* 171(11):3125–3141
- Brace WF, Byerlee JD (1966) Stick-slip as a mechanism for earthquakes. *Science* 153(3739):990–992
- Brantut N, Viesca RC (2015) Earthquake nucleation in intact or healed rocks. *J Geophys Res* 120(1):191–209
- Brantut N, Baud P, Heap MJ, Meredith PG (2012) Micromechanics of brittle creep in rocks. *J Geophys Res* 117:B08412
- Byerlee J (1978) A review of rock mechanics studies in the United States pertinent to earthquake prediction. *Pure Appl Geophys* 116:586–602
- Cao W, Shi JQ, Si G, Durucan S, Korre A (2018) Numerical modelling of microseismicity associated with longwall coal mining. *Int J Coal Geol* 193:30–45
- Charles RJ (1958) Static fatigue of glass I. *J Appl Phys* 29(11):1549–1553
- Colombero C, Comina C, Vinciguerra S, Benson PM (2018) Microseismicity of an unstable rock mass: from field monitoring to laboratory testing. *J Geophys Res* 123(2):1673–1693
- Crampin S, Evans R, Atkinson BK (1984) Earthquake prediction: a new physical basis. *Geophys J Int* 76:147–156
- Crampin S, Gao Y, Bukits J (2015) A review of retrospective stress-forecasts of earthquakes and eruptions. *Phys Earth Planet Inter* 245:76–87
- Daniels KE, Hayman NW (2008) Force chains in seismogenic faults visualized with photoelastic granular shear experiments. *J Geophys Res* 113:B11411
- Dieterich JH (1979a) Modeling of rock friction 1. Experimental results and constitutive equations. *J Geophys Res* 84(B5):2161–2168
- Dieterich JH (1979b) Modeling of rock friction 2. Simulation of preseismic slip. *J Geophys Res* 84(B5):2169–2175
- Douglas A, Beavan J, Wallace L, Townend J (2005) Slow slip on the northern Hikurangi subduction interface New Zealand. *Geophys Res Lett* 32:L16305
- Dragoni M, Lorenzano E (2017) Dynamics of a fault model with two mechanically different regions. *Earth Planets Space* 69:145
- Dragoni M, Tallarico A (2016) Complex events in a fault model with interacting asperities. *Phys Earth Planet Inter* 257:115–127
- Fossen H, Schultz RA, Torabi A (2011) Conditions and implications for compaction band formation in the Navajo Sandstone, Utah. *J Struct Geol* 33(10):1477–1490
- Grgic D, Amitrano D (2009) Creep of a porous rock and associated acoustic emission under different hydrous conditions. *J Geophys Res* 114:B10201
- Griffith WA, Rosakis A, Pollard DD, Ko CW (2009) Dynamic rupture experiments elucidate tensile crack development during propagating earthquake ruptures. *Geology* 37(9):795–798
- Hardebeck JL, Nazareth JJ, Hauksson E (1998) The static stress change triggering model: constraints from two southern California aftershock sequences. *J Geophys Res* 103(B10):24427–24437
- Hatzfeld D, Ziazia M, Kementzetzidou D, Hatzidimitriou P, Panagiotopoulos D, Makropoulos K, Deschamps A (1999) Microseismicity and focal mechanisms at the western termination of the North Anatolian Fault and their implications for continental tectonics. *Geophys J Roy Astron Soc* 137(3):891–908
- Healy D, Jones RR, Holdsworth RE (2006) Three-dimensional brittle shear fracturing by tensile crack interaction. *Nature* 439:64–67

- Houston H (2015) Low friction and fault weakening revealed by rising sensitivity of tremor to tidal stress. *Nat Geosci* 8(5):409–415
- Ikari MJ, Marone C, Saffer DM, Kopf AJ (2013) Slip weakening as a mechanism for slow earthquakes. *Nat Geosci* 6(6):468–472
- Katz O, Reches Z (2004) Microfracturing damage and failure of brittle granites. *J Geophys Res* 109(B1):B01206
- Leeman JR, Saffer DM, Scuderi MM, Marone C (2016) Laboratory observations of slow earthquakes and the spectrum of tectonic fault slip modes. *Nat Commun* 7:11104
- Li XZ, Shao ZS (2016) Investigation of macroscopic brittle creep failure caused by microcrack growth under step loading and unloading in rocks. *Rock Mech Rock Eng* 49(7):2581–2593
- Li XZ, Shao ZS, Fan LF (2016) A micro–macro method for predicting the shear strength of brittle rock under compressive loading. *Mech Res Commun* 75:13–19
- Li XZ, Qi CZ, Shao ZS, Qu XL (2018a) Static shear fracture influenced by historic stresses path and crack geometries in brittle solids. *Theor Appl Fract Mech* 96:64–71
- Li XZ, Qi CZ, Shao ZS (2018b) A microcrack growth-based constitutive model for evaluating transient shear properties during brittle creep of rocks. *Eng Fract Mech* 194:9–23
- Lockner DA, Byerlee JD, Kuksenko V, Ponomarev A, Sidorin A (1991) Quasi-static fault growth and shear fracture energy in granite. *Nature* 350:39–42
- Martin CD, Chandler NA (1994) The progressive fracture of Lac du Bonnet granite. *Int J Rock Mech Min Sci Geomech Abstr* 31(6):643–659
- Miura K, Okui Y, Horii H (2003) Micromechanics-based prediction of creep failure of hard rock for long-term safety of high-level radioactive waste disposal system. *Mech Mater* 35(3):587–601
- Niemeijer AR, Vissers RLM (2014) Earthquake rupture propagation inferred from the spatial distribution of fault rock frictional properties. *Earth Planet Sci Lett* 396:154–164
- Noda H, Lapusta N (2013) Stable creeping fault segments can become destructive as a result of dynamic weakening. *Nature* 493(7433):518–521
- Ohnaka M (1995) A shear failure strength law of rock in the brittle-plastic transition regime. *Geophys Res Lett* 22(1):25–28
- Pearson C (1981) The relationship between microseismicity and high pore pressures during hydraulic stimulation experiments in low permeability granitic rocks. *J Geophys Res* 86(B9):7855–7864
- Pei Y, Paton DA, Knipe RJ, Wu K (2015) A review of fault sealing behaviour and its evaluation in siliciclastic rocks. *Earth-Sci Rev* 150:121–138
- Rice JR (1993) Spatio-temporal complexity of slip on a fault. *J Geophys Res* 98(B6):9885–9907
- Rice JR, Ruina AL (1983) Stability of steady frictional slipping. *J Appl Mech* 50:343–349
- Ruff L (1992) Asperity distributions and large earthquake occurrence in subduction zones. *Tectonophysics* 211:61–83
- Ruina A (1983) Slip instability and state variable friction laws. *J Geophys Res* 88(B12):10359–10370
- Scholz CH (1998) Earthquakes and friction laws. *Nature* 391(6662):37–42
- Scholz CH, Sykes LR, Aggarwal YP (1973) Earthquake prediction: a physical basis. *Science* 181:803–810
- Shelly DR, Peng Z, Hill DP, Aiken C (2011) Triggered creep as a possible mechanism for delayed dynamic triggering of tremor and earthquakes. *Nat Geosci* 4(6):384–388
- Somerville P, Irikura K, Graves RW, Sawada S, Wald DJ, Abrahamson NA, Kagawa YIT, Smith N, Kowada A (1999) Characterizing crustal earthquake slip models for the prediction of strong ground motion. *Seismol Res Lett* 70(1):59–80
- Svetlizky I, Fineberg J (2014) Classical shear cracks drive the onset of dry frictional motion. *Nature* 509(7499):205
- Tueckmantel C, Fisher QJ, Knipe RJ, Lickorish H, Khalil SM (2010) Fault seal prediction of seismic-scale normal faults in porous sandstone: a case study from the eastern Gulf of Suez rift, Egypt. *Mar Pet Geol* 27(2):334–350
- Xiao YX, Feng XT, Chen BR, Feng GL, Yao ZB, Hu LX (2017) Excavation-induced microseismicity in the columnar jointed basalt of an underground hydropower station. *Int J Rock Mech Min Sci* 97:99–109
- Yu J, Liu GY, Cai YY, Zhou JF, Liu SY, Tu BX (2020) Time-dependent deformation mechanism for swelling soft-rock tunnels in coal mines and its mathematical deduction. *Int J Geomech* 20(3):04019186
- Zhao XG, Cai M (2010) A mobilized dilation angle model for rocks. *Int J Rock Mech Min Sci* 47(3):368–384